Enhanced Kinetochore Detection During Mitotic Human Cell Division using CFAR

Abdullahi Daniyan*†, Alessio V. Inchingolo†, Andrew McAinsh†, and Nigel Burroughs*
*Mathematics Institute, University of Warwick, Coventry, CV4 7AL. United Kingdom
†Centre for Mechanochemical Cell Biology and Division of Biomedical Sciences,
Warwick Medical School, University of Warwick, CV4 7AL. United Kingdom

Email: abdullahi.daniyan@warwick.ac.uk, a.d.mcainsh@warwick.ac.uk, n.j.burroughs@warwick.ac.uk

***Abstract*—In this paper, we present an innovative application of the Constant False Alarm Rate (CFAR) algorithm, traditionally utilized in radar signal processing, to enhance the accuracy and reliability of kinetochore (KT) tracking in live-cell lattice light-sheet microscopy (LLSM) imaging of human cells during the mitotic phase of cell division. Fluorescently labelled KTs appear as spots in diffraction-limited light microscopy. Traditional KT detection methods, such as adaptive thresholding, often struggle with the dynamic and noisy backgrounds of cells, leading to less efficient KT identification. By adapting the CFAR algorithm to the specific challenges of KT detection in 3D, we present a method that offers improved precision and stability in detecting KTs across different stages of mitosis. The performance of the CFAR-KT method was rigorously compared to the adaptive thresholding approach across a cohort of 31 cells, with results highlighting CFAR-KT's enhanced detection efficiency. Despite a slightly lower mean detection count compared to the adaptive method, the CFAR-KT method achieved lower false positives and a higher success rate in tracking KTs over the duration of the cell division process, underscoring its effectiveness in capturing the dynamics of KTs.**

I. Introduction

Cell division is a fundamental biological process where a cell (typically) divides into two near-identical daughter cells. It is essential for life, underpinning growth, repair, and reproduction in all organisms [1], whilst errors in cell division result in diseases such as cancer. Cell division is split into phases: S phase, where the genome is duplicated, *mitosis* where the duplicated chromosomes are segregated into two nuclei, and finally, cytokinesis, where the cell divides into two daughter cells. Duplicated chromosomes remain paired through mitosis as so-called sister chromatids. The cell constructs the spindle, a microtubule-based machine organised around 2 spindle poles that facilitates the accurate descent of a complete set of chromosomes to each daughter cell. Microtubules are dynamic filaments that are a fundamental part of the cellular cytoskeleton. They are important in internal cell transport, cell movement and cell division. During mitosis, which is also split into phases, each chromatid of a pair is captured by respective spindle poles (prometaphase), the pair aligns at the cell mid-plane (metaphase), and once all chromosomes are attached/aligned, the sister pairing is dissolved and the duplicated chromosomes are separated and moved to opposite spindle poles (anaphase), Figure 1. The kinetochore (KT), a multi-protein complex on each chromatid, facilitates the connection between chromosomal DNA and microtubules. KTs generate and control the forces driving chromosome movements, ensuring precise attachment to spindle microtubules, sister alignment, and movement of chromosomes during mitosis [2].

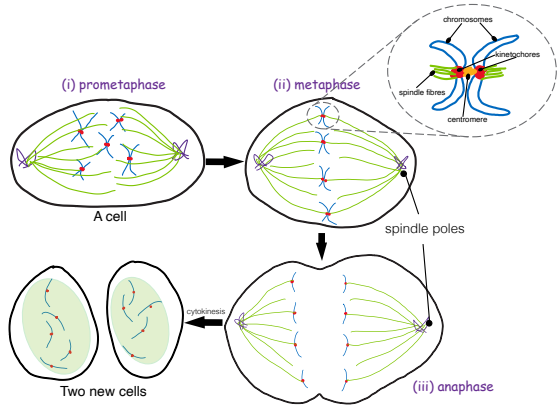

Fig. 1. Schematic of mitosis showing (i) prometaphase where the spindle self assembles and chromosomes are captured, (ii) metaphase where sister chromatids align to the cell's mid-plane forming the metaphase plate, and (iii) anaphase where sister chromatids are segregated to opposite spindle poles. Cytokinesis then ensues, forming 2 daughter cells. KTs are shown in red.

Advances in live cell imaging, in particular lattice light-sheet microscopy (LLSM), have revolutionized the ability to visualise cellular events with unprecedented clarity over extended periods of time at high time resolution [3]. Live imaging of the KT allows tracking of chromosome dynamics throughout cell division, providing a detailed life history across mitosis and invaluable insights into both typical and atypical behaviours. However, achieving the full potential of this approach requires an accurate and reliable spot detection step, a prerequisite for effective tracking and analysis. Current methodologies for KT detection primarily rely on traditional image processing techniques, which still grapple with issues of sensitivity and specificity, particularly in the noisy backgrounds characteristic of cellular environments. These limitations underscore the need for innovative approaches that can enhance detection accuracy, thereby improving the reliability of subsequent analyses of cell division and genetic integrity.

In this context, the application of a Constant False Alarm Rate (CFAR) algorithm, a detection technique pioneered in radar signal processing, offers a promising solution. CFAR, designed to maintain a constant false alarm rate despite varying background noise levels, provides a robust framework for detecting objects of interest in complex, dynamic scenarios [4]. When signals are corrupted by non-homogeneous noise, the CFAR detector is widely preferred for peak detection in radar systems [5]. By adapting CFAR to the domain of computational biology, specifically for the detection of KTs in LLSM movies, this work leverages the algorithm's inherent capability to discriminate between true signals and background noise to improve detection outcomes.

This paper presents a novel application of the CFAR technique to improve KT detection, demonstrating its effectiveness through increased performance and accuracy in analysing LLSM movies of human cells during mitotic cell division. This interdisciplinary approach not only offers a more reliable method for KT analysis but also exemplifies the potential of engineering solutions in addressing complex biological problems.

II. Related Work

Over the years, several detection techniques have been developed to enhance the accuracy and reliability of identifying cellular structures in microscopy images. The evolution of these techniques reflects our growing understanding of the complexities involved in live-cell imaging. This section reviews notable advances in this field.

The unimodal thresholding algorithm [6] offers a bilevel thresholding approach for images with unimodal distributions. This algorithm finds an optimal threshold by drawing a line from the peak to the higher end of the histogram and selecting the point that maximizes the distance from this line to the histogram curve as the threshold.

The wavelet method [7], based on the multiscale product of wavelet-transformed subband images, enhances multiscale features corresponding to spots while minimizing noise. Thresholding non-significant coefficients combines information across different resolution levels to identify spots distinctively.

The adaptive thresholding method [8] differentiates true particles from noise by analyzing a particle's displacement between consecutive frames. This algorithm sets a global intensity threshold to balance the detection of particles across frames [9], aiming to minimize the difference between particle clouds from one frame to the next and to maximize the acceptance of true particles [10]. The algorithm begins with background level estimation through a 3-D Gaussian filter, subtraction from each frame, and recording the intensities of local maxima. An exponential function, fitted to mean frame intensities to correct for photobleaching, adjusts the intensities of local maxima. Particle detection within a frame involves local maxima whose corrected intensities meet or exceed a threshold, optimized globally to balance position consistency and a penalty for strict thresholds using a pattern search algorithm.

Comparatively, while unimodal thresholding offers speed but limited robustness to background fluorescence, the wavelet method effectively reduces false positives in noisy conditions despite being slower and requiring fine-tuning. Although susceptible to missed detections, adaptive thresholding applies a global threshold considering all movie frames, unlike the fixed frame-by-frame threshold of the unimodal and wavelet methods. These methods are tuned on a population of spots, and so are, in our context, cell-level-based thresholding methods. The proposed CFAR method, by employing a dynamic particle-specific threshold, allows for the local environment of each KT, thus offering distinct advantages by adjusting for the local noise. The method promises greater robustness against background fluorescence and noise, thereby reducing false positives in noisy images.

III. The Proposed CFAR-Based Kinetochore (CFAR-KT) Detection Method for LLSM Cell Data

In this section, we begin by outlining the context and characteristics of data obtained from LLSM imaging of human retinal pigment epithelial cells (RPE1). We then provide an overview of the traditional 1-D CFAR algorithm as applied in radar signal processing, highlighting its principles and effectiveness in detecting objects against variable backgrounds. Building on this, we introduce our innovative approach, adapting the CFAR technique to develop the CFAR-KT method, specifically tailored for precise and reliable kinetochore detection in live imaging.

A. Context

The general context is the analysis of fluorescently labelled proteins that cluster tightly into diffraction-limited spots. We analyse human RPE1 cells with endogenously labelled kinetochores (Ndc80-eGFP, [11]). LLSM imaging of live cells labelled with multiple flourophores gives a 4-Dimensional (4-D) dataset per channel, where each channel corresponds to a distinct fluorescent marker. For example, besides the KT channel, there could be channels for microtubules and DNA, providing a detailed view of these structures within the context of KT movements. The term 4-D refers to the inclusion of time (T) alongside three spatial dimensions (X, Y, Z), capturing the dynamics of cellular processes over time through various frames and slices.

In these 4-D datasets, each frame captures a moment in time across the cell's 3-D volume. In the KT channel, KTs appear as Gaussian spots distributed across the cell volume, reflecting their positions and movements throughout cell division. Figure 2 shows a 3-D volume of a typical LLSM imaged RPE1 cell. This is a single channel image where the KTs are flourescently labelled, flourescence is in the green part of the spectrum (488 nm laser). Figure 3 shows a maximum intensity z-axis projection of an LLSM RPE1 imaged cell.

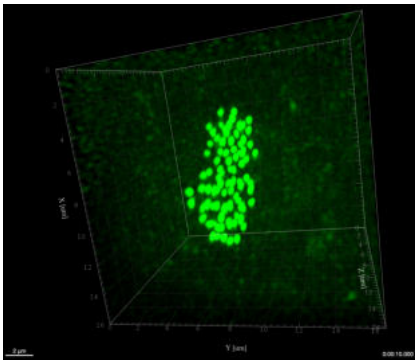

Fig. 2. A 3-D volume image of KTs at a single time-point from LLSM imaging of a RPE1 cell during mitosis. KT are endogenously labelled with eGFP, [11].

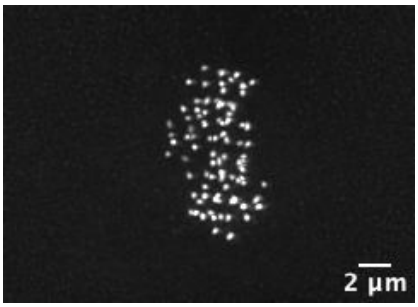

Fig. 3. A typical single time-point maximum intensity z-projection of an LLSM imaged RPE1 cell showing KTs during mitosis (same cell as in Figure 2, frame 10).

B. Traditional 1-D CFAR

In radar signal processing, a radar antenna is used for transmitting and receiving radar signals, Figure 4(a). When the radar signal encounters a target, a time-delayed and attenuated version of the original signal is received back at the radar transmitter, Figure 4(b). The time delay of the reflected echo enables the determination of the target(s)' range. To detect the

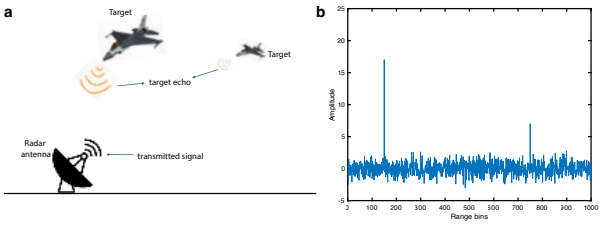

Fig. 4. (a) Radar and targets (b) Target return echo

presence of an echo, CFAR utilises a window, Figure 5, to define a dynamic detection threshold. The CFAR algorithm adjusts the detection threshold based on the local noise level, maintaining a constant false alarm rate amidst varying noise levels. This is accomplished by the designation of a reference bin, referred to as the bin under test (BUT), denoted by S, surrounded by guard bins (N_G) and training bins (N_t), where N_G and N_t represent the number of guard and training bins, respectively. The average noise level is calculated by averaging the signal levels in the reference cells. Guard cells are excluded to prevent the target from influencing the noise estimate. The detection threshold is then computed by multiplying the average noise level by a scaling factor k, which is set based on the desired false alarm rate.The signal level of the BUT is compared against the computed threshold. If the signal level exceeds the threshold, a target is declared; otherwise, it is considered noise.

Mathematically, the process can be summarized for a BUT at position i as follows:

- Let N_{lead} and N_{lag} be the number of leading and trailing training bins, respectively such that $N_t = N_{lead} + N_{lag}$.
- Let S_i be the signal level of the BUT.
- Calculate the average noise level $\bar{N}$ as:

$$E = \frac{\sum_{j=i-N_{lead}}^{i-1} X_j + \sum_{j=i+1}^{i+N_{lag}} X_j}{N_{lead} + N_{lag}} \tag{1}$$

where X_j represents the signal level in the jth training bin. The detection threshold T is then:

$$T = E \cdot k \tag{2}$$

where k is the scaling factor. A target is detected if $S_i > T$. The exact formulation of k depends on the desired false alarm rate and the statistics (statistical model) of the background noise, often assumed to be Gaussian or Rayleigh distributed. Applying the CFAR detector to the target echo depicted in Figure 4(b) results in the detection threshold illustrated in Figure 6, where the CFAR detector threshold is indicated in red and a fixed threshold in blue. This approach successfully identifies the two targets.

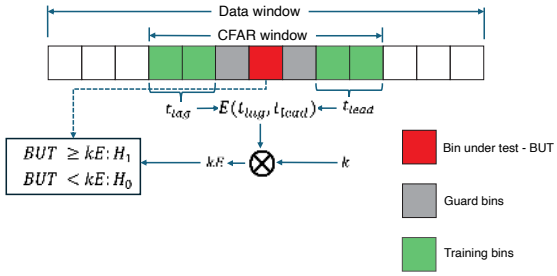

Fig. 5. 1-D CFAR Window. This figure depicts the configuration and operational logic of the 1-D Constant False Alarm Rate (CFAR) detection algorithm. The CFAR window includes the bin under test (BUT), guard bins, and training bins. The training bins (green) are used to estimate the noise level $E(t_{lag}, t_{lead})$, excluding the influence of the signal in the guard bins (gray) and the BUT (red). The estimated noise level is then multiplied by a scaling factor k to determine the detection threshold kE. The signal level in the BUT is compared against this threshold to decide whether a target is present (H_1) or not (H_0).

C. The Proposed CFAR-KT

To enable KT detection in the 3-D volumes captured by LLSM, (X, Y, and Z dimensions), we generalise the 1-D CFAR methodology to a 3-D context. We utilise a 3-D CFAR window that can be moved through the cell's 3-D volume at

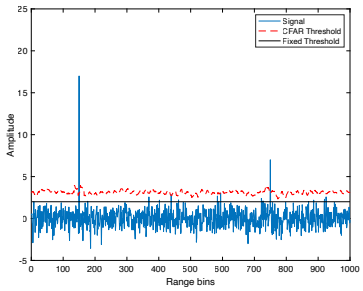

Fig. 6. Received radar target signal showing different detection thresholds

each time-point, thus maintaining a constant false alarm rate across the data cube by adapting the detection threshold to the local noise. This approach enables the detection of KTs in each frame throughout an LLSM movie sequence.

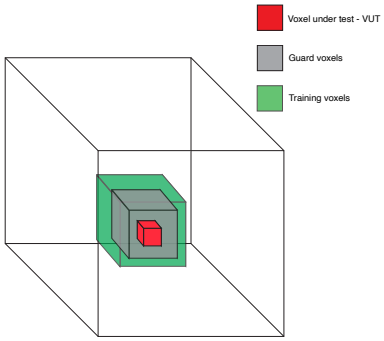

Fig. 7. 3-D CFAR window

Specifically, a CFAR window that moves through the cell is defined, consisting of noise-estimating training voxels (TV), guard voxels to prevent the target influencing local noise estimation, and the voxel under test (VUT) itself (Figure 7). The (local) noise level is then computed using training voxels around the VUT in all dimensions, excluding guard voxels. A detection threshold is computed by multiplying the average noise level by a scaling factor (α), its value being set based on the desired false alarm rate, thus adjusting the threshold to local noise levels. Lastly, the VUT's signal level is compared against the threshold, with signals exceeding the threshold marked as potential KTs. For a given VUT at position (i, j, k) within a 3-D grid,

- Let the signal levels within the grid be $X_{x,y,z}$, where x, y, and z index the three spatial dimensions.
- Define the numbers of guard voxels (N_g) and training voxel (N_t) around the VUT, distributed in all three dimensions around the VUT.
- The average noise level E (local to the VUT) is computed by averaging the signal levels in the training voxels, excluding the guard voxels and the VUT:

$$E = \frac{\sum_{(x,y,z)\in TV} X_{x,y,z}}{N_t} \tag{3}$$

where the summation is over the training voxels (set TV) only. Note that the training voxels (TV) vary with the VUT. The detection threshold T is then determined by:

$$T = E \cdot \alpha \tag{4}$$

A KT is detected at the VUT if the signal level at voxel (i, j, k), $X_{i,j,k} > T$.

IV. Experimental Results

To evaluate the efficacy of our proposed method, we analysed 31 human RPE1 cells imaged with LLSM during mitosis. Kinetochores are fluorescently labelled and the cell is imaged in a single channel; each movie consists of at least 241 frames with a frame interval of 2.07 seconds, a timing that captures the dynamics of kinetochore movements in mitosis. During mitosis, RPE1 cells have a normal complement of 46 chromosomes; thus there are 92 kinetochores (KTs) per cell to be detected and tracked in mitosis.

CFAR-KT was integrated into the existing KiT software for kinetochore tracking [8]. We compared its performance against the adaptive thresholding KT detection method currently available in KiT [8]. KiT is a MATLAB-based software. Our analysis was carried out on a Macbook Pro M1 Max machine with MATLAB version R2022b. The LLSM imaging data was processed according to the pipeline shown in Figure 8.

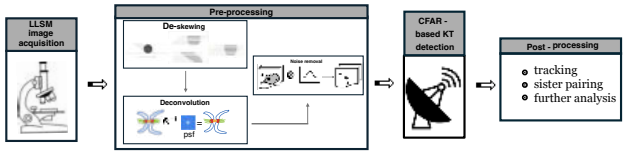

Fig. 8. RPE1 cell imaging and processing pipeline.

To illustrate CFAR-KT, we first discuss its performance on a typical cell, termed cell A for simplicity. Cell A had 350 frames beginning from late prometaphase to late anaphase, Figure 1. We then extend the analysis to the entire cohort of 31 cells, providing a comprehensive comparison between the proposed method and the adaptive thresholding approach outlined in [8]. The choice of the adaptive thresholding method as a benchmark is based on previous studies that have highlighted its effectiveness over both the unimodal thresholding [6] and the wavelet methods [7] in KT detection. This comparison demonstrates the enhanced accuracy and reliability of our method in detecting and tracking KTs during mitosis.

A. Analysis on a single Cell

Figure 9 illustrates the performance of CFAR-KT detection compared to the adaptive thresholding detection method for cell A during mitosis. Both methods detect close to the expected 92 KTs, the adaptive thresholding method averaging 91.2 KTs per frame and the CFAR-KT method averaging 90 KTs per frame. However, CFAR-KT is more consistent across

the movie, with standard deviations of 0.14 for the adaptive thresholding method and 0.05 for the CFAR-KT method.

Figure 10 visually examines the detected spots in typical frames. Despite the adaptive method's generally higher detection count, its accuracy and precision are questioned. A z-axis projection of cell A's first frame is shown in Figure 10(a), including a magnified section with overlaid detections. The adaptive method's 94 detections include 4 false positives, marked by cyan arrows in the zoomed view.

At frame 142, Figure 10(b), both methods record 90 KT detections. However, the CFAR-KT method demonstrates superior precision in pinpointing KT centroid, as shown by the cyan "+" marks at the center of each KT spot. In contrast, the adaptive method's detections, marked by red circles, occasionally deviate from the KT centers, as indicated by white arrows in the zoomed view.

In anaphase, Figure 10(c), the CFAR-KT method consistently detects 90 KTs, whereas the adaptive method misses one, with 89 detections. The overlooked KT is highlighted by a yellow arrow in the magnified section.

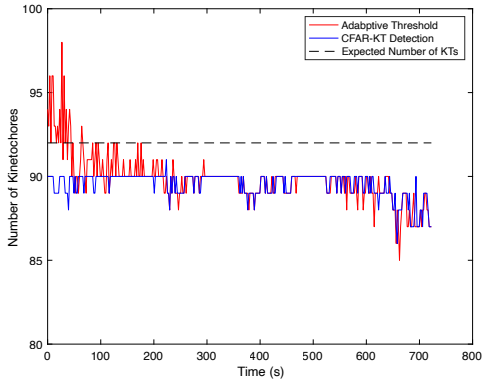

Fig. 9. Comparison of KT detection counts by method for cell A

KT tracks were generated from the detected spots for each method using the KiT software, [8]. Barcode plots show when individual tracks were present throughout the movie, Figure 11; subfigure (a) corresponds to the adaptive method, and (b) to the CFAR-KT method. Despite detecting fewer KTs, the CFAR-KT method results in longer, fuller tracks, underscoring the precision and reliability of its detections compared to the higher but less accurate counts from the adaptive method.

In all, while the CFAR-KT method may report slightly fewer detections per frame on average for cell A, its detections are more accurate and reliable, enhancing tracking performance. This evidence supports the proposed method's advantage in kinetochore detection during cell division.

B. Performance on 31 cells

We compared the performance of both the CFAR-KT detection and adaptive thresholding methods across a cohort of 31 cells undergoing mitosis. The average number of spots detected by both methods across the 31 cells is shown in Figure 12, shown over the first 241 frames.

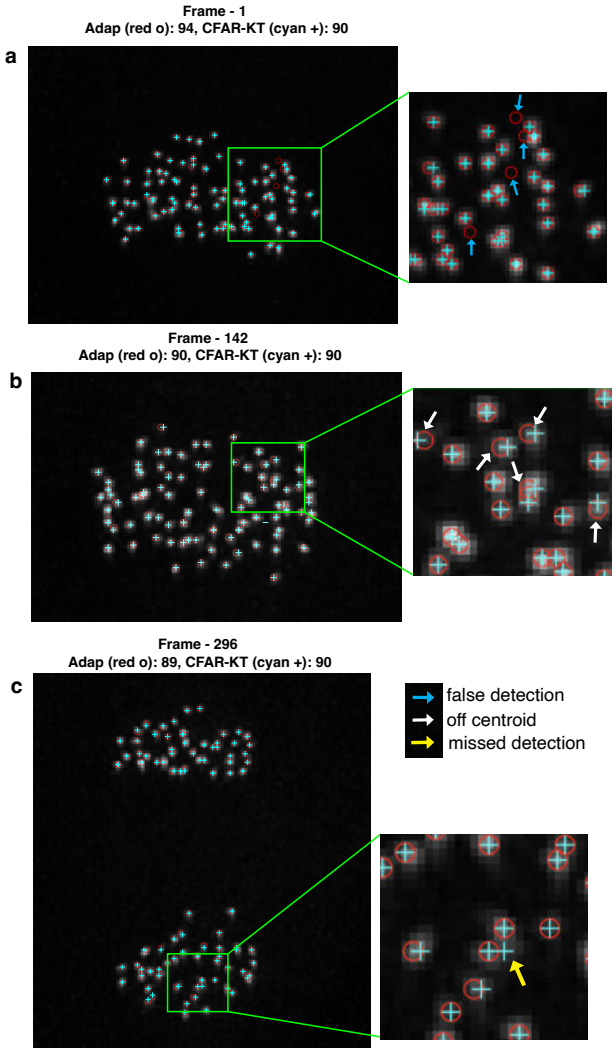

Fig. 10. Adaptive thresholding (red circle) and CFAR-KT-based (cyan +) detections overlaid on z-projected images of three frames from cell A during mitosis. The cyan, white and yellow coloured arrows highlight false detections, off-centroid and missed detections, respectively.

Both methods detect close to the expected 92 KTs, with the CFAR-KT having a standard deviation of 0.03 and the adaptive thresholding method 0.11. As for cell A, the adaptive thresholding method has a slightly higher detection count, averaging around 91.7 KTs per frame, with a similar profile to that seen in the single cell with an initially higher count in prometaphase. In contrast, the CFAR-KT method's detections are more consistent, with fewer fluctuations, averaging around 91 KTs per frame. Despite the seemingly higher detection count by the adaptive method, this does not necessarily indicate superior performance, echoing findings from the analysis of cell A.

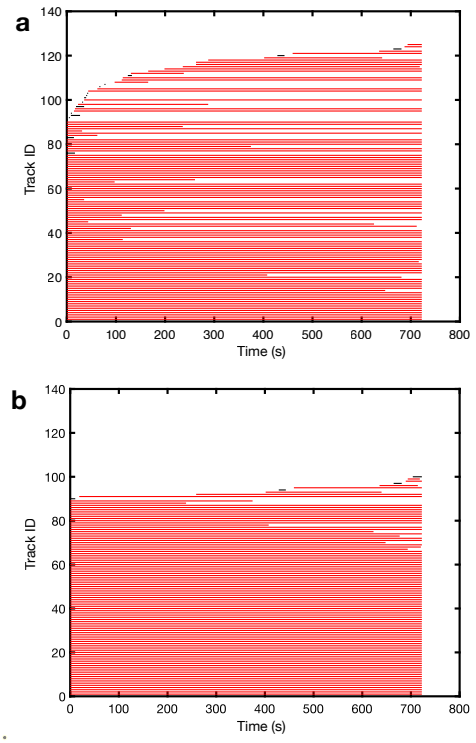

Fig. 11. Barcode plot showing birth and death of detected and tracked kinetochores from cell A. (a) Adaptive thresholding method (b) CFAR-KT method. Red lines represent KTs tracked for at least 10% of the movie length, and black lines denote shorter-lived tracks.

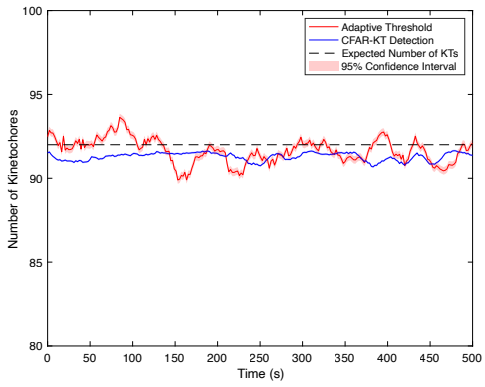

Fig. 12. KT detection method comparison averaged over 31 cells (first 241 frames). The expected number of KTs (92) is indicated by the dashed black line. The adaptive thresholding method is shown by the blue line, while the CFAR-KT method is indicated by the red line. The shaded areas depict the standard deviation for each method, highlighting the CFAR-KT method's robustness in providing reliable KT detection.

Table I provides a quantitative comparison. The adaptive method's average detection rate per cell was 91.73 equating to an impressive 99.7% accuracy when compared to the expected number of KTs in a cell. However, this translated into only 67.4% of KT tracks lasting for at least 75% of the movie length. Conversely, the CFAR-KT method, with its slightly lower detection accuracy of 98.96% when compared to the expected number of KTs in a cell, resulted in a significantly higher number of tracks (87.02%) lasting 75% of the movie.

These results confirm not only the CFAR-KT method's ability to provide accurate and reliable detection in a single cell, as demonstrated with cell A but also its consistently improved performance across a group of cells undergoing mitosis.

TABLE I
KINETOCHORE DETECTION AND TRACKING PERFORMANCE IN 31 HUMAN RPE1 CELLS

Method	Avg. KTs detected per cell	Tracked KTs with 75% track length
Adaptive thresholding	91.73 (99.70%)	1922 (67.39%)
CFAR-KT	91.05 (98.96%)	2482 (87.02%)

Table II compares the mean and standard deviation of track lengths for both KT detection detection methods across the 31 cells. The CFAR-KT method shows a higher mean track length and lower standard deviation, indicating more consistent and reliable KT tracking compared to the adaptive thresholding method. A chi-squared test comparing the proportion of tracks with at least 75% length between the adaptive and CFAR-KT methods yielded a p-value of 0.000353. This indicates a statistically significant difference between the two methods, with the CFAR-KT method showing a higher proportion of longer tracks.

TABLE II
COMPARISON OF MEAN AND STANDARD DEVIATION OF TRACK LENGTHS

Method	Mean Track Length (s)	Std Dev of Track Length (s)
Adaptive Thresholding	251.64	140.41
CFAR-KT	513.87	64.70

V. CONCLUSION

In this study, we introduced and evaluated a novel Constant False Alarm Rate (CFAR)-based kinetochore (KT) detection method and incorporated it into the live-cell KT tracking pipeline of KiT, [8]. Through quantitative comparison with an existing adaptive thresholding detection method across a cohort of 31 human RPE1 cells undergoing mitosis, our results demonstrate that CFAR-KT is superior, both as regards accuracy of detection on individual images, Figure 10, and delivers superior downstream tracks with fewer breaks, Figure 11, Table I and Table II.

Our analyses, grounded in both individual cell evaluations and broader population studies, reveal that while both CFAR-KT and adaptive thresholding methods detect close to the expected kinetochore count, the CFAR-KT method provides a more consistent detection rate with fewer errors. Importantly, the CFAR-KT method's slight reduction in raw detection numbers did not detract from its performance. Instead, it

translated into a significantly higher tracking success rate, underscoring the method's ability to accurately reflect the true presence and dynamics of kinetochores within the cells.

The implications of these findings extend beyond the technical achievements of improving detection algorithms. By enabling more accurate and reliable kinetochore tracking, CFAR-KT opens new avenues for understanding the complex mechanisms of mitosis and the roles that KTs play in genetic stability and cell division. This, in turn, can inform future research into cellular dysfunctions and diseases linked to errors in cell division, such as those that occur in cancer.

Although adapted to KT detection and tracking, CFAR, with its emphasis on allowing for local levels of noise, is generally applicable to the detection of any cellular spot-like structure in any imaging modality.

ACKNOWLEDGMENT

This work was supported by the Biotechnology and Biological Sciences Research Council with grant number BB/R009503/1 and also supported by a Wellcome Senior Investigator Award to A.N. (grant 106151/Z/14/Z). The Lattice Light Sheet Microscope Facility was established at Warwick with a Wellcome Trust Multi-user Equipment grant (grant 208384/Z/17/Z). We thank the Computational and Microscopy Development Unit (CAMDU) for support with lattice light sheet microscopy.

REFERENCES

[1] D. Mazia, "Cell Division," *Scientific American*, vol. 189, no. 2, pp. 53–63, 1953.

[2] A. D. McAinsh and A. L. Marston, "The Four Causes: The Functional Architecture of Centromeres and Kinetochores," *Annual review of genetics*, vol. 56, pp. 279–314, 2022.

[3] B.-C. Chen, W. R. Legant, K. Wang, L. Shao, D. E. Milkie, M. W. Davidson, C. Janetopoulos, X. S. Wu, J. A. Hammer III, Z. Liu *et al.*, "Lattice Light-sheet Microscopy: Imaging Molecules to Embryos at High Spatiotemporal Resolution," *Science*, vol. 346, no. 6208, p. 1257998, 2014.

[4] M. Richards, J. Scheer, and W. Holm, "Principles of Modern Radar Vol I Basic Principles. 2010."

[5] M. Weiss, "Analysis of Some Modified Cell-averaging CFAR Processors in Multiple-target Situations," *IEEE Transactions on Aerospace and Electronic Systems*, no. 1, pp. 102–114, 1982.

[6] P. L. Rosin, "Unimodal Thresholding," *Pattern recognition*, vol. 34, no. 11, pp. 2083–2096, 2001.

[7] J.-C. Olivo-Marin, "Extraction of Spots in Biological Images Using Multiscale Products," *Pattern recognition*, vol. 35, no. 9, pp. 1989–1996, 2002.

[8] J. W. Armond, E. Vladimirou, A. D. McAinsh, and N. J. Burroughs, "KiT: a MATLAB Package for Kinetochore Tracking," *Bioinformatics*, vol. 32, no. 12, pp. 1917–1919, 2016.

[9] P. K. Sahoo, S. Soltani, and A. K. Wong, "A Survey of Thresholding Techniques," *Computer vision, graphics, and image processing*, vol. 41, no. 2, pp. 233–260, 1988.

[10] C. Torre-Ferrero, J. R. Llata, L. Alonso, S. Robla, and E. G. Sarabia, "3D Point Cloud Registration Based on a Purpose-Designed Similarity Measure," *EURASIP Journal on Advances in Signal Processing*, vol. 2012, no. 1, pp. 1–15, 2012.

[11] O. Sen, J. U. Harrison, N. J. Burroughs, and A. D. McAinsh, "Kinetochore Life Histories Reveal an Aurora-B-dependent Error Correction Mechanism in Anaphase," *Developmental cell*, vol. 56, no. 22, pp. 3082–3099, 2021.